

Active tectonics in Taiwan: insights from a 3-D viscous finite element model

Yujun Sun · Mian Liu · Shuwen Dong · Huai Zhang · Yaolin Shi

Received: 25 November 2013 / Accepted: 15 November 2015 / Published online: 11 December 2015
© The Author(s) 2015. This article is published with open access at Springerlink.com

Abstract Taiwan is a young orogenic belt with complex spatial distributions of deformation and earthquakes. We have constructed a three-dimensional finite element model to explore how the interplays between lithospheric structure and plate boundary processes control the distribution of stress and strain rates in the Taiwan region. The model assumes a liberalized power-law rheology and incorporates main lithospheric structures; the model domain is loaded by the present-day crustal velocity applied at its boundaries. The model successfully reproduces the main features of the GPS-measured strain rate patterns and the earthquake-indicated stress states in the Taiwan region. The best fitting model requires the viscosity of the lower crust to be two orders of magnitude lower than that of the upper crust and lithospheric mantle. The calculated deviatoric stress is high in regions of thrust faulting and low in regions of extensional and strike-slip faulting, consistent with the spatial pattern of seismic intensity in Taiwan.

Keywords Taiwan · Stress · Strain rate · FEM model · Earthquake

1 Introduction

The Taiwan Island is located at the convergent boundaries between the Eurasian and the Philippine Sea plates (Fig. 1). To its northeast, the Philippine Sea plate subducts beneath the Eurasian Plate along the Ryukyu trench. To its south, the Eurasian Plate thrusts under the Philippine Sea plate along the Manila trench. As a young orogenic belt, Taiwan experiences intensive active tectonic motion, as indicated by the global positioning system (GPS) measurements and seismicity (Tsai et al. 1977; Yu et al. 1997; Lin 2002) (Fig. 1). Data from the Taiwan GPS Network show that the Philippine Sea plate moves toward Chinese mainland margin at 82 mm/a with the azimuth of 306° (Yu et al. 1997). The GPS velocity jumps by 30 mm/a across the Longitudinal Valley Fault (LVF), which is the suture zone of active plate collision in Taiwan (Yu et al. 1997; Chang et al. 2000; Yu and Kuo 2001). The GPS data also show rotation at both tips of the Taiwan collision belt (clockwise in NE Taiwan, anticlockwise in SW Taiwan) (Ching et al. 2007; Angelier et al. 2009), probably related to the escape tectonics of Taiwan (Lacombe et al. 2001).

Seismic activity is intense in Taiwan, which is highlighted by the 1999 M_w 7.6 Chi-Chi (Ji-Ji) earthquake that killed more than 2000 people and caused over \$10 billion property damage (Wang and Shin 1998; Ma et al. 1999; Shin et al. 2000; Hsu et al. 2007). Focal mechanism solutions are consistent with the tectonic transition from oblique subduction along the Luzon arc to collision in much of the Taiwan island (Kao et al. 1998, 2000).

Y. Sun
Institute of Geomechanics, Chinese Academy of Geological Sciences, Beijing 100081, China

M. Liu · H. Zhang · Y. Shi (✉)
Key Laboratory of Computational Geodynamics, Chinese Academy of Sciences, Beijing 100049, China
e-mail: shiy1@ucas.ac.cn

M. Liu
Department of Geological Sciences, University of Missouri, Columbia, MO 65211, USA

S. Dong
Chinese Academy of Geological Sciences, Beijing 100037, China

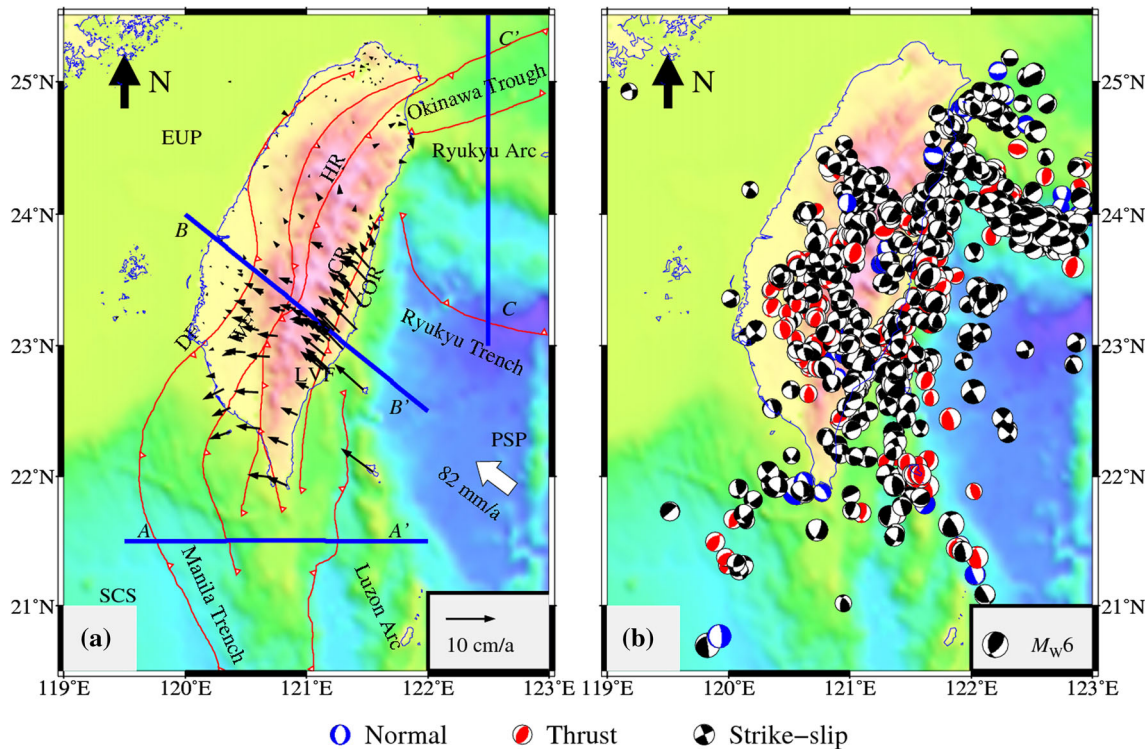


Fig. 1 **a** Tectonic features in the Taiwan region. The red lines indicate major faults. The tick marks show the dip direction of the fault surfaces. The black arrows indicate the GPS velocity in the Taiwan region (Yu et al. 1997). EUP Eurasian Plate, SCS South China Sea, PSP Philippine Sea plate, DF deformation front, WF Western Foothill, HR Hsuehshan Range, CR Central Range, COR Coastal Range, LVF Longitudinal Valley Fault. **b** The seismic distribution in the Taiwan region. Focal mechanism solutions indicate the events with magnitude $M_w \geq 4.0$ and focal depths ≤ 50 km from 1995 to 2010 (data from Broadband Array in Taiwan for Seismology (BATS))

The GPS data and earthquake focal mechanism have been used to constrain two-dimensional (2-D) geodynamic models of regional tectonics in Taiwan (Hu et al. 1996, 1997, 2001). These models are helpful for understanding crustal deformation and seismicity in the Taiwan region. However, given the complex plate interactions in this region, it remains unclear whether the active tectonic in Taiwan is primarily controlled by plate boundary forces or if the lithospheric structure plays a significant role. In this study, we constructed a fully 3-D finite element model for the Taiwan Island and surrounding regions. Using the GPS and seismic data as the primary constraints, we explored how tectonic boundary conditions and rheological structures control the active tectonics in the Taiwan region.

2 Numerical model

2.1 Governing equations and rheology

The mechanical equilibrium for steady-state lithospheric deformation can be expressed as

$$\sigma_{ij,j} + f_i = 0 \quad i, j = 1, 2, 3, \quad (1)$$

where σ_{ij} is the stress tensor, and f_i is the gravitational body force. Because this study focuses on the present-day lithospheric deformation, we assume relative plate motion to be the main tectonic loading and ignore gravitational body force from topographic loading, hence $f_i = 0$ (Li et al. 2009).

For the short-term crustal or lithospheric deformation and interaction of rigid plates, the elastic rheology is reasonable because of relative small deformation (Richardson 1978; Coblenz and Richardson 1996). But for the purposes of describing its large-scale and long-term deformation, the continental lithosphere should be regarded as a continuum, obeying a Newtonian or a power-law rheology (England and McKenzie 1982; England and Houseman 1986; Houseman and England 1986). The steady-state deformation of the lithosphere is probably close to that of a power-law fluid, with the strain rate being proportional to the cubic power of stress (Brace and Kohlstedt 1980; Kirby and Kronenberg 1987; Liu and Yang 2003). The power-law rheology can be linearized by using an effective viscosity:

$$\bar{\sigma} = \eta_{\text{eff}} \bar{\dot{\epsilon}}, \quad (2)$$

where

$$\bar{\sigma} = \sqrt{3J_2} = \sqrt{\frac{3}{2}S_{ij}S_{ij}}, \tag{3}$$

$$\sigma_{ij} = S_{ij} + \frac{1}{3}\sigma_{ij}\delta_{ij}, \tag{4}$$

where $\bar{\sigma}$ is the Von Mises stress or the effective stress, S_{ij} is the deviatoric stress tensor, J_2 is the second invariant of deviatoric stress, and δ_{ij} is the Kröner delta.

$$\bar{\dot{\epsilon}} = \sqrt{\frac{4}{3}J'_2} = \sqrt{\frac{2}{3}\dot{\epsilon}_{ij}\dot{\epsilon}_{ij}}, \tag{5}$$

$$\dot{\epsilon}_{ij} = \dot{\epsilon}_{ij} + \frac{1}{3}\dot{\epsilon}_{ij}\delta_{ij}. \tag{6}$$

$\bar{\dot{\epsilon}}$ is the effective strain rate, $\dot{\epsilon}_{ij}$ is the strain rate tensor, $\dot{\epsilon}_{ij}$ is the deviatoric strain rate, and J'_2 is the second invariant of deviatoric strain rate. The relationship between strain rate tensor and velocity vector v_i is

$$\dot{\epsilon}_{ij} = \frac{1}{2}(v_{i,j} + v_{j,i}). \tag{7}$$

We define the effective viscosity η_{eff} as (Shi and Cao 2008; Sun et al. 2013)

$$\eta_{\text{eff}} = \frac{1}{2} \left(\frac{\bar{\dot{\epsilon}}}{A} \right)^{\frac{1}{n}} e^{\frac{E}{nRT}} \bar{\dot{\epsilon}}^{-1}, \tag{8}$$

where n is the power-law exponent, A is a scaling factor, E is the activation energy, R is the universal gas constant, and T is the absolute temperature. The effective viscosity is strain rate dependent. However, because here we consider only the background steady-state strain rate, we treat the effective viscosity as a constant. We built the numerical codes using the commercial finite element package FEPG (the website is www.ectec.asia), which has been used to study many problems in geological sciences (Liu et al. 2000; Liu and Yang 2003; Sun et al. 2014).

2.2 Model setup

The model domain encompasses the region of 20.5°N–25.5°N, 119°E–123°E, which covers the Taiwan Island and surrounding regions, including the plate boundaries (Fig. 2). The model domain is 100 km in depth. The three-dimensional lithospheric structure is very complex in Taiwan area (Kim et al. 2005; Wu et al. 2007; Kuo-Chen et al. 2012). In this study, for simplification, the crustal thickness is based on the Crust2.0 model (<http://igppweb.ucsd.edu/~gabi/rem.html>), assuming Airy isostasy and using the topography data from ETOPO2v2g (<http://www.ngdc.noaa.gov/mgg/global/relief/ETOPO2/ETOPO2v2-2006/ETOPO2v2g/>). The densities of the crust and mantle are taken to be 2700 and 3300 kg/m³, respectively (Yen et al. 1995, 1998; Chi et al. 2003).

Faults play an important role in the tectonic deformation. The GPS observation shows that there are jumps of velocity and strain rate across the major faults, especially for the suture zones (Chang et al. 2003). From the east to west, Taiwan Island can be divided into several tectonic units. The Coastal Range (CR) to the east represents the northern Luzon Arc accreted to the collided margin. The Longitudinal Valley Fault (LVF) is the suture zone between the Philippine Sea plate and Eurasian plate. The west of it is the Central Range (CR) and Hsuehshan Range (HR). Western Foothills (WF), which is a non-metamorphic foreland and thrust belt, results from the compression of Peikang High. Further west, the Coastal Plain (CP) lies at the Deformation Front (DF) between the frontal thrust units and Peikang High (Angelier et al. 2009; Mouthereau et al. 2009) (Figs. 1, 3). There are also many small faults among these major faults. But the strain rate distribution derived from the GPS observation shows that high strain rate is mainly distributed along the major faults (Chang et al. 2003). That means the major faults allocate the crustal deformation. Considering the effect of these faults on the deformation, we have included the major faults in our model (Fig. 2), which are simulated as weak zones with relatively low effective viscosities. Each of them has a dip angle (30°–90°, the representation of the dipping planes is limited by the grid resolution) and strike variations (Figs. 1, 2). We assume that the faults extend through the upper crust. The subduction zones are also simulated as weak zones; their depth profiles are based on seismicity (Wu et al. 1997; Wang and Shin 1998; Kao et al. 2000).

The numerical model has 274,930 finite element nodes and 512,784 prism elements, which are formed by mapping the surface triangle element along the depth direction. The size of each element is approximately 5 km (Fig. 2).

2.3 Boundary conditions and model parameters

As a first-order approximation, we assume that lithospheric blocks move coherently in the vertical directions. Hence, the surface velocity measured by the GPS is extrapolated to depth. These velocities are relative to the stable Chinese continental margin (Fig. 1a). Hence in our model, the northern and western sides of the Eurasian plate are fixed in the horizontal directions and free in the vertical direction (Fig. 2). The southern and western sides of the model domain are imposed with velocity boundary conditions based on the GPS observation. The velocity magnitude and direction varies linearly (shown in Fig. 3). Free-slip boundary condition is imposed on the southwestern boundary of the model (Fig. 2), but we imposed proper velocities on the northeastern margin of the model domain to reflect the back-arc spreading there as indicated by GPS

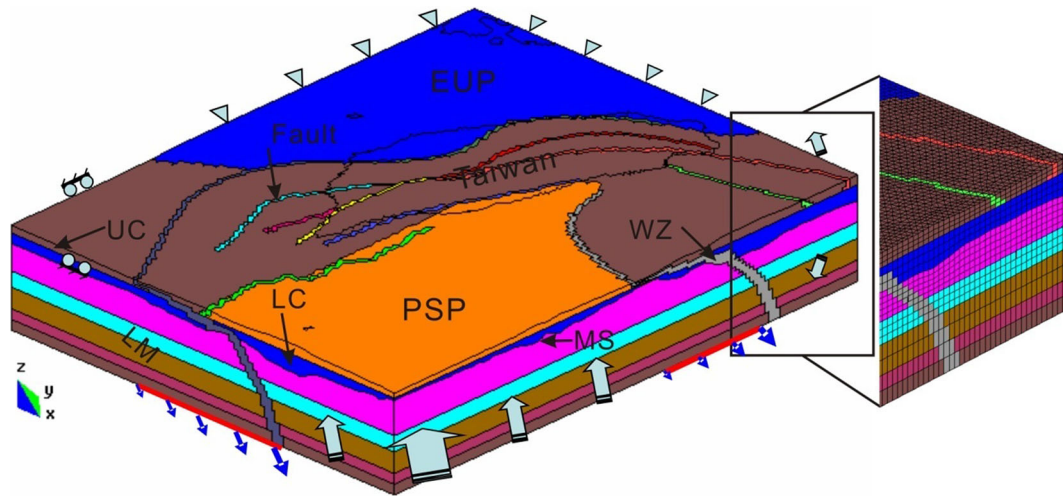


Fig. 2 Finite element model and the boundary conditions. Different material parameters (effective viscosity) are assigned to different parts, shown in different colors (see Fig. 4). Zoom-in figure shows the finite element mesh used in the model. *EUP* Eurasian plate, *PSP* Philippine Sea plate, *UC* upper crust, *LC* lower crust, *LM* lithospheric mantle, *WZ* weak zone, *MS* Moho surface

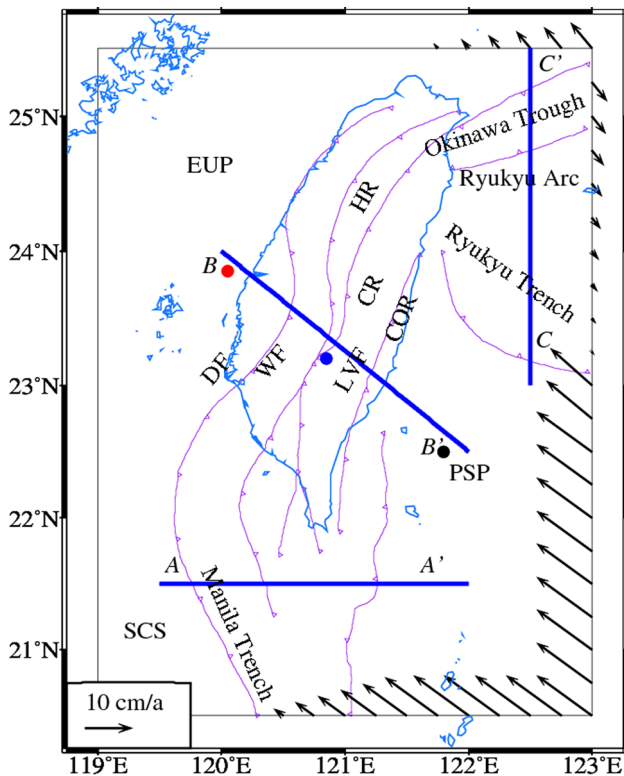


Fig. 3 The velocity boundary condition imposed on the sides of the model domain. *EUP* Eurasian Plate, *SCS* South China Sea, *PSP* Philippine Sea plate, *DF* Deformation Front, *WF* Western Foothill, *HR* Hsuehsan Range, *CR* Central Range, *COR* Coastal Range, *LVF* Longitudinal Valley Fault. Viscosity structure is shown for the color dots (Fig. 4)

data (Hu et al. 2001; Kubo and Fukuyama 2003; Angelier et al. 2009). The Earth surface of the whole model domain is full free boundary condition.

The boundary conditions on the bottom of the model domain cannot be directly constrained. The simplest one is a free-slip bottom, but it maybe improper near the two subduction zones, where we used a velocity boundary condition (the red lines on the bottom of the model in Fig. 2) in alternative models. The relative velocity along the Manila and Ryukyu subduction plate is 101.6 and 83.2 mm/a, respectively. We assumed 57° dipping for both subduction interfaces (Shiono and Sugi 1985; Wang and Shin 1998). The velocity imposed on the bottom of the model is consistent with the relative velocity along the dipping direction.

The whole domain is divided into four layers. Each of them is assigned with an effective viscosity. The total lithospheric integrated strength (LIS) suggests there is a weak lower crust in the hinterland, which correlates very well with the earthquake depth-frequency distribution (Ma and Song 2004). In this study, the upper crust of Philippine Sea plate, Eurasian plate, and Collision zone are assigned different viscosities, respectively. But for the lower crust and lithospheric mantle in the model, the same viscosity is given. The values are based on rheological structure for this region, which is calculated based on the parameter of lithology, temperature, and strain rate (Ma and Song 2004; Sun et al. 2011) (Fig. 4).

3 Results

We carried out a suite of forward numerical experiments to explore the effects of different boundary conditions and the viscosity structures, using the GPS data and the stress states indicated by earthquake focal mechanisms as the primary constraints.

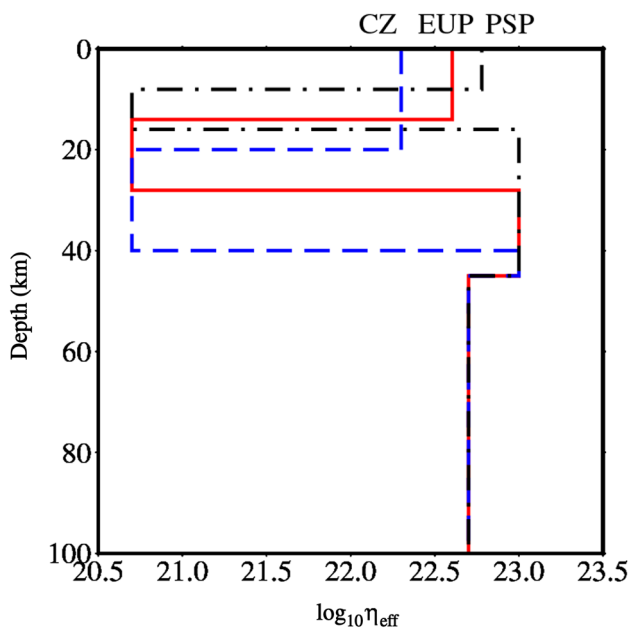


Fig. 4 The schematic diagram for effective viscosity profiles. *EUP* Eurasian Plate, *PSP* Philippine Sea plate, *CZ* Collision Zone (brown domain between EUP and PSP in Fig. 2). Three profiles in this figure represent the viscosity structure for three specific sites (Fig. 3) because the crustal thickness in our model is variable (Fig. 2). *Blue dashed line* represents the collision zone. *Red solid line* denotes the Eurasian plate. *Black dot-dashed line* shows the Philippine Sea plate

3.1 Horizontal distribution of velocity, strain rate, and stress

Our calculated surface velocities are generally comparable with the GPS site velocities in the Taiwan region (Fig. 5a), indicating the overall control of plate boundary motion on crustal deformation in the Taiwan region. To fit the GPS velocity changes over major faults across the Taiwan orogen (Fig. 5b), we need to lower the effective viscosity of the fault zones by two orders of magnitude (for the LVF) and one order of magnitude (for other faults) relative to that of the neighbour crust. The velocity jumps across these faults are associated with localized high strain rates (Fig. 5c). The maximum compressive strain rate is up to $10^{-6}/a$ along the LVF in eastern Taiwan and up to $10^{-7}/a$ across other faults in the central range and western foothill of Taiwan Island. These results suggest that weak fault zones are the primary control of strain localization and partitioning within the Taiwan orogen.

The misfits between the simulated velocity and GPS-measured velocity mainly exist at the southwestern and northeastern parts of the Taiwan Island (Fig. 5a). Particularly, the anticlockwise rotation of the GPS velocity cannot be reproduced in the model if the Philippine Sea plate is

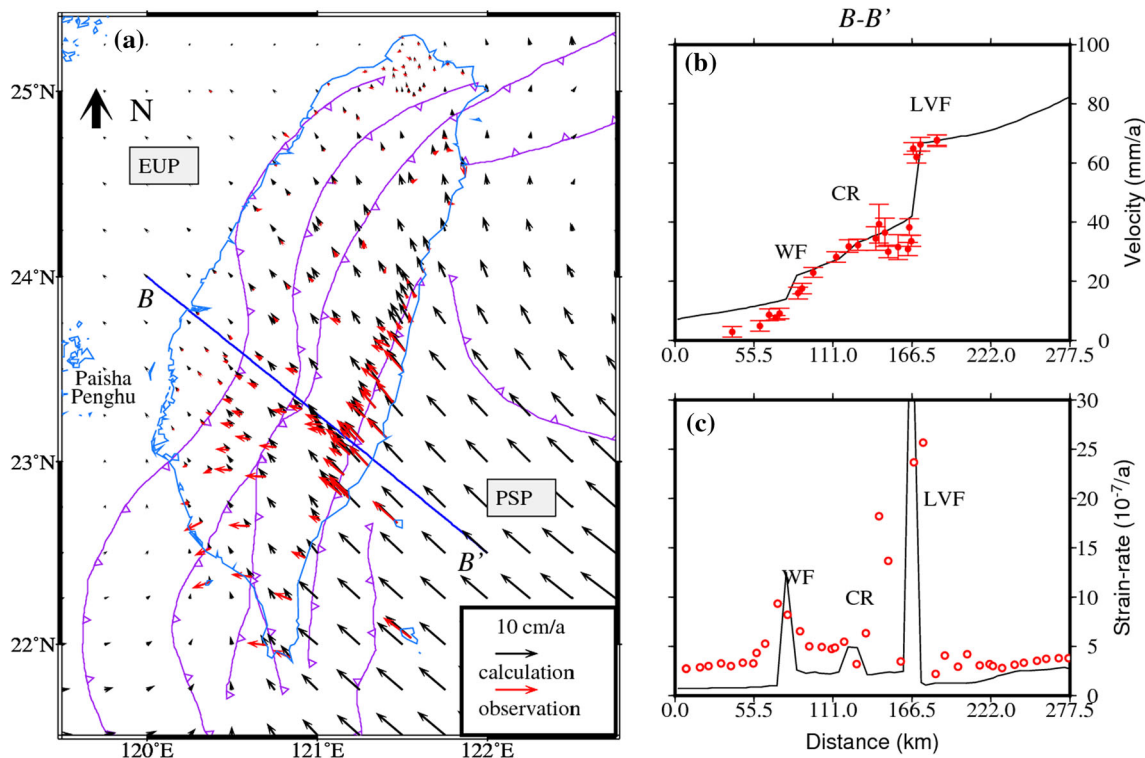


Fig. 5 **a** Comparison of the calculated surface velocity (*black arrows*) and the GPS velocity relative to Paisha, Penghu (Yu et al. 1997). **b** The *black solid line* indicates the calculated surface velocity and the *red error bars* represent the GPS velocity along the profile *BB'*; **c** The *black solid line* and *red circles* indicate the simulated strain rate (maximum principle strain rate) and the GPS-derived strain rate along the profile *BB'*, respectively (Chang et al. 2003). *WF* Western Foothill, *CR* Central Range, *LVF* Longitudinal Valley Fault. The value in *x-axis* (**b**, **c**) indicate the distance from the site *B* along the profile *B-B'*

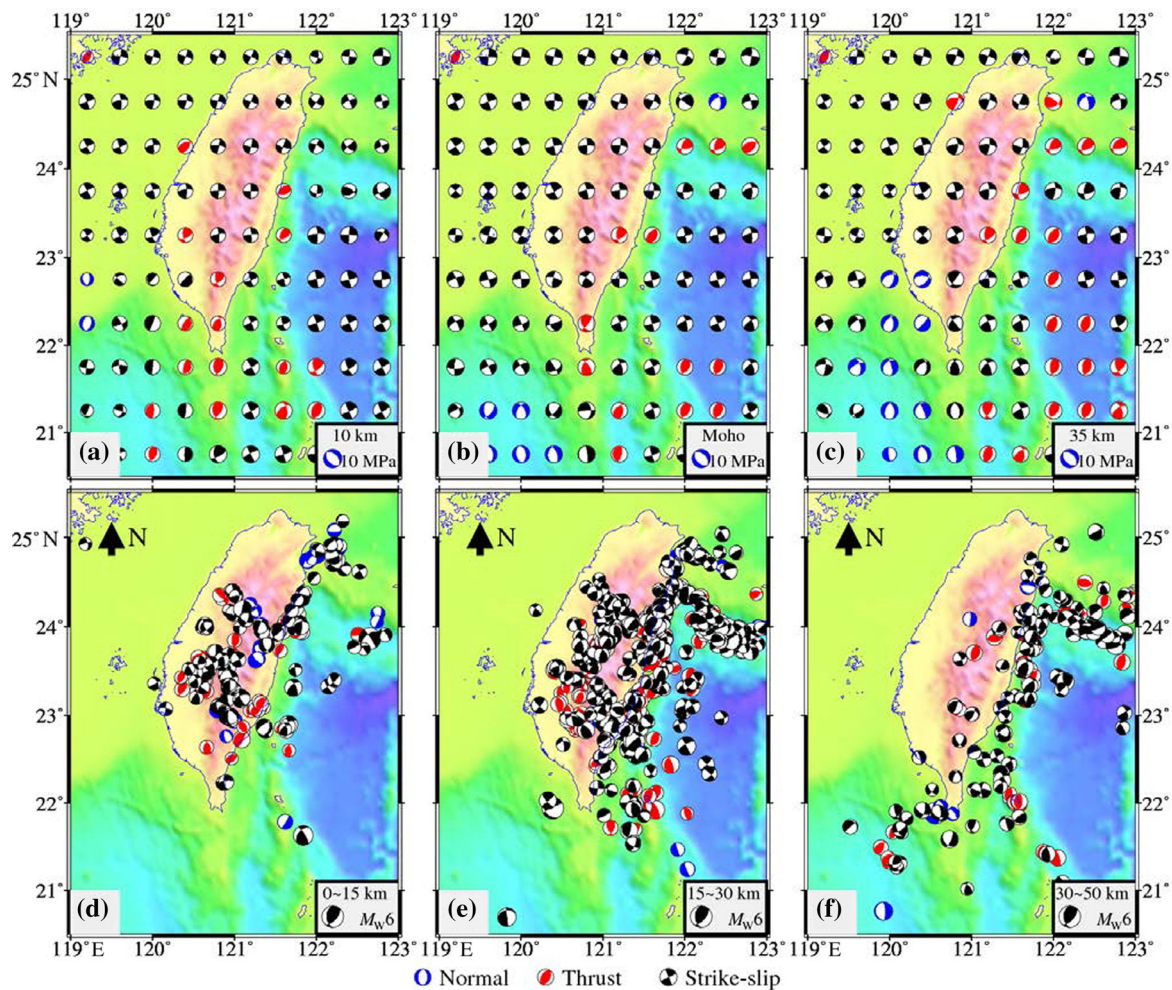


Fig. 6 Calculated deviatoric stress in the horizontal direction at various depths (a–c) and earthquake focal mechanism solutions (d–f). The three-dimensional stress states are shown by the stereographic lower-hemisphere projection similar to that for earthquake focal mechanism solution. The maximum (σ_1) and minimum (σ_3) principle stress bisect the *white and colored quadrants*, respectively. They are similar to the P and T axes in earthquake focal mechanism. Focal mechanism solutions are for events with magnitude $M_w \geq 4.0$ from 1995 to 2010. Depth numbers in the *lower right corner* represent the specific depths for the calculation deviatoric stress (a–c) and the range of focal depths (d–f)

assigned with a uniform direction of motion. This suggests that the direction of plate convergence probably varies along the plate boundary.

In Fig. 6, we compare the calculated three-dimensional stresses with earthquake focal mechanism solutions. The stress regimes of the whole region, based on seismicity and focal mechanism solutions, can be divided into four sub-systems: the Ryukyu subduction in the northeast, the Philippine Sea plate boundary system in the southeast, the South China Sea in the southwest, and the northwest overthrust bending system in the northeast (Wang and Shin 1998). The earthquakes in the southwestern part of the Okinawa Trough indicate extension, the extensional stress state can be reproduced in our model by imposing velocity boundary conditions simulating back-arc spreading in this area (Kao et al. 1998; Kubo and Fukuyama 2003). The

Philippine Sea plate boundary system is characterized by intense seismicity with predominantly thrust events, especially along the LVF. Our model predicts both thrusting and strike-slip stress here. In the Manila subduction system, the seismic pattern changes with depth. Near the surface the stress state is predominantly compressive, which changes to extensional with normal-faulting earthquake beneath the Moho (Figs. 6, 8). This change can be reproduced in the model by lowering the effective viscosity of the lower crust by two-order magnitude relative to that of the upper crust and lithospheric mantle. This implies that those deep normal-fault earthquakes in that region may originate from the upper mantle because the low viscosity of lower crust make the deformation decoupling between the upper crust and upper mantle (Kaus et al. 2009; Wu et al. 2009; Sun et al. 2011). In the northwest overthrust

bending system, the predicted stress state is consistent with the predominantly strike-slip faulting suggested by earthquake focal mechanism solutions. Observation stress obtained from the focal mechanism is complicated, which is influenced by the regional tectonic structure and lithology. In the shallow layers (<10 km), the calculated results is not consistent well with the observation stress. For instance, many normal faults are developed in the East Central Range. A possible reason is gravitational collapse, which is similar with the extension in the center of Tibetan plateau (Liu and Yang 2003). But the focus of this study is on the present-day lithospheric deformation, we assume relative plate motion to be the main tectonic loading and ignore gravitational body force from topographic loading. Thus, the shallow calculated stresses may have differences with the focal mechanism.

3.2 Vertical variation of strain rate and stress

The 3-D model allows us to examine variations of velocity, strain rate, and stress with depth. Here, we show these variations along three profiles (Fig. 1) across the Manila subduction zone, the Taiwan collision zone, and Ryukyu

subduction zone, respectively. First, we show the maximum shear strain rate and dilatation rate along these profiles (Fig. 7). The maximum shear strain rate γ is defined as $\gamma = |\dot{\epsilon}_{\max} - \dot{\epsilon}_{\min}|$, (9)

where $\dot{\epsilon}_{\max}$ and $\dot{\epsilon}_{\min}$ are the maximum and the minimum principle strain rate, respectively, so γ indicates the intensity of deformation. The dilatation rate is defined as $\theta = (\dot{\epsilon}_{\max} + \dot{\epsilon}_{\min})/2$. (10)

Positive θ indicates that the deformation is dominated by elongation or extension, while negative θ is for compressive deformation. The velocity and strain rate varied with depth is shown in Fig. 7. The deviatoric stress and earthquake focal mechanism (within the range of 1°) along these three profiles are shown in Fig. 8.

Across the Manila subduction zone (profile A-A'), high shear strain concentrates along the subduction zone, which is modeled as a low-viscosity weak zone (Fig. 7a, b). Assuming a weak lower crust allows the compressive upper crust to be partially decoupled from the lithospheric mantle, where the down-going and bending of the plate cause extensional stress in the upper lithospheric mantle

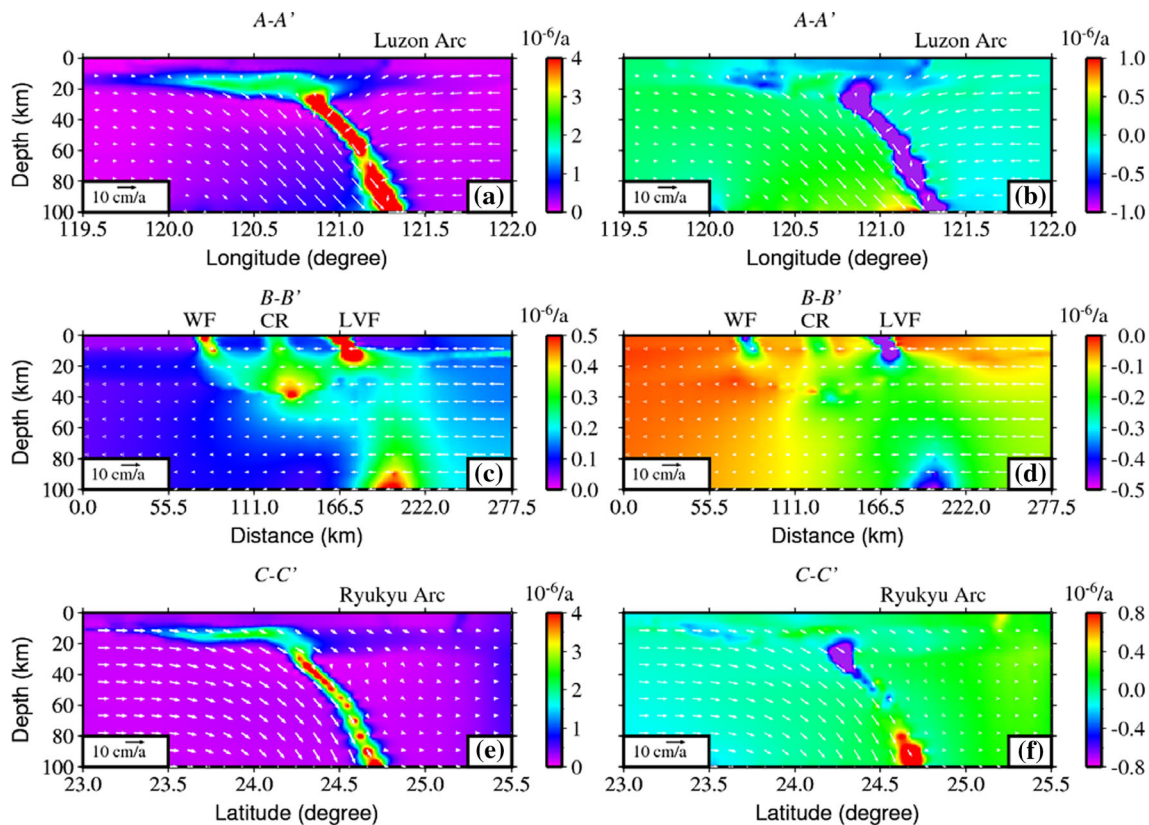


Fig. 7 The maximum shear strain rate γ (left panels) and dilatation rate θ (right panels) along the profiles crossing the Manila subduction zone (A-A'), the Taiwan collision zone (B-B'), and the Ryukyu subduction zone (C-C'). Positive dilatation rates indicate extension, negative for compression. Arrows are the velocity vectors along these profiles. WF Western Foothill, CR Central Range, LVF Longitudinal Valley Fault

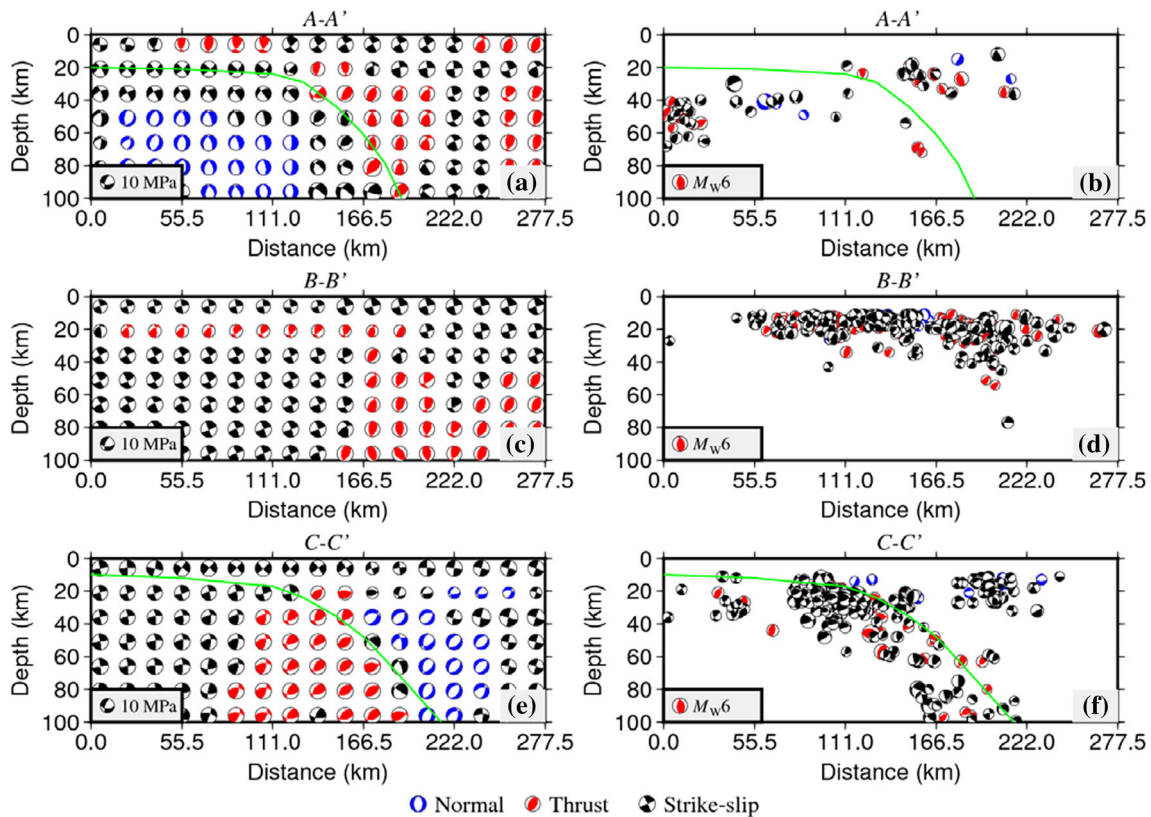


Fig. 8 Comparison of deviatoric stress (*left panels*) and earthquake focal mechanism solutions (*right panels*) along Manila subduction zone (*A-A'*), the Taiwan collision zone (*B-B'*), and the Ryukyu subduction zone, (*C-C'*). The events shown are those within the range of 1° to each profile. The *green lines* indicate the location of the subduction plate interface

(Fig. 8a). This condition is necessary to account for the changing stress states with depth in this region as indicated by earthquake focal mechanism (Fig. 8b).

Across the Taiwan Island (the *B-B'* profile), the dilatation rate is dominantly negative because of the compressive stress resulting from the collision. The highest strain rate is near the LVF, central range, and western foothill (Fig. 7c, d).

The calculated strain rate pattern across the Ryukyu subduction system (the *C-C'* profile) is similar to that of the Manila subduction zone (Fig. 7e, f). The mainly difference is that there is positive dilatational strain (extension) in the northern part of the *C-C'* profile (right side of Fig. 7e, f) near the Okinawa trough, where back-arc spreading occurs. Accordingly, the predicted stress shows extension in this region, which is consistent with some of the normal-fault events in the upper crust but not the deeper events (Fig. 8f).

4 Discussion

We have built a fully three-dimensional finite element model to simulate the active tectonics of the Taiwan region. As for any 3-D numerical models, the more realistic

representation of the Earth system comes with a price, which is the increased uncertainty associated with more parameters and boundary conditions. In the following, we discuss parameter selection and the impacts on model results in three aspects: model structure, material properties, and boundary conditions.

The complex plate configurations and tectonic patterns in the Taiwan region account for the complex patterns of the GPS site velocities. Our model only considers the first-order geometry of the major faults. Nonetheless, by lowering the effective viscosity in the fault zones, we were able to reproduce much of the surface strain rates and their spatial variations as indicated by the GPS velocities. The results require the LVF to be much weaker than other faults in the region.

The calculated strain rate shows shortening at the subducting plate boundaries. Our results indicate that a better-fitted stress state requires a weaker lower crust and an oceanic crust being able to be dragged down by the subducting slab. Other studies also proposed that the weak lower crust exists in the Taiwan area (Mouthereau and Petit 2003; Zhou et al. 2003; Ma and Song 2004; Kaus et al. 2009).

The boundary conditions employed in our model are based on the GPS-measured plate kinematics, which are similar to that used by previous 2-D plane models (Hu et al. 2001). But in this study, we are mainly interested in the spatial patterns of stress and strain rates. Even though the plate velocities may alter over long geological time (Liu et al. 2000), the relative plate moving direction could be presumably stable in the past few million years (Demets et al. 1994).

The model results also depend on the bottom boundary conditions in our 3-D model. Models that involve no subduction usually assume the base conditions to be free-slip in the horizontal direction and fixed in the vertical direction. However, in the Taiwan region, there are two subduction systems. Without these subduction zones in the model, we are unable to generate the stress variations with depth, especially the deep normal-faulting earthquakes in the southwestern part of the Taiwan region. In our model, we varied the magnitudes of the vertical velocity imposed on the lower boundary to satisfy the stress constrains from earthquake focal mechanism solutions. Including subduction in the model also improves fit to the surface velocity

and strain rate (Fig. 9). The results show that using the free-slip boundary (FSB) on the bottom of the model produces a poor fit between the observed and computed velocity. Along the profile *BB'*, the magnitude of the computed velocity is larger than the observed velocity. When the velocity boundary (VB) on the bottom of the model domain simulates subduction, it produces a better fit to the surface velocity.

5 Conclusions

With the 3-D FEM model, we explored how the plate boundary processes and lithospheric structure control active tectonics in the Taiwan region. We find that while the overall crustal deformation is controlled by the plate boundary processes, the distribution of strain within the Taiwan orogen is largely controlled by weak faults zones. In particular, the LVF zone should be two orders of magnitudes weaker than that of the neighbor crust. Our results also require the effective viscosity of the lower crust under the Taiwan orogen to be more than two orders of

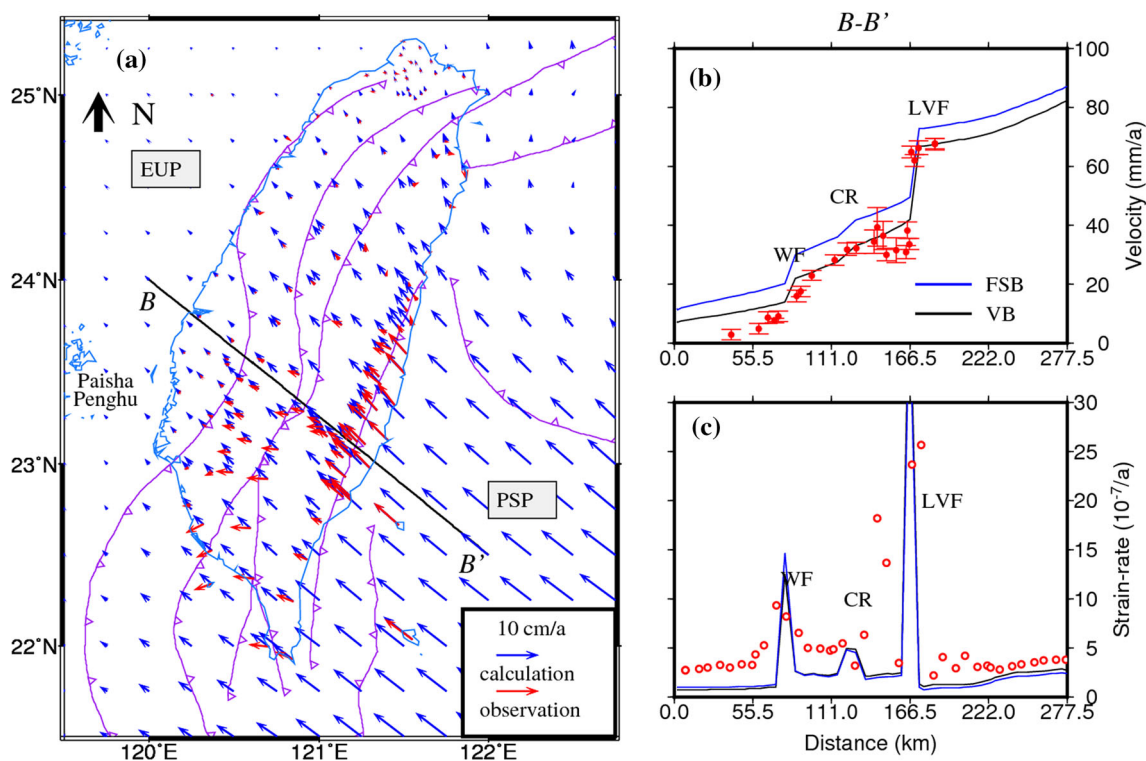


Fig. 9 The effects of 3-D boundary condition on the results **a** Comparison of the calculated surface velocity (blue arrows) with free-slip boundary on the bottom of the model and the GPS velocity relative to Paisha, Penghu (Yu et al. 1997). **b** Blue and black solid lines are the calculated surface velocity with free-slip and velocity boundary along the subduction zones, respectively. The red error bars represent the GPS velocities along the profile *BB'*; **c** Blue and black solid dash indicate the calculated strain rate (maximum principle strain rate) with free-slip and velocity boundary, respectively. The red circles represent strain rate calculated by the GPS observation along the profile *BB'* (Chang et al. 2003). WF Western Foothill, CR Central Range, LVF Longitudinal Valley Fault, FSB free-slip boundary on the bottom of the model, VB velocity boundary on the bottom of the model

magnitudes lower than that of upper crust and lithospheric mantle. Existence of this weak lower crust is needed to account for variation of stress states with depth as indicated by earthquake focal mechanisms.

While the entire Taiwan region is predominantly compressive because of the plate convergence, our model predicts extensional stress in the depth range of mantle lithosphere under the South China Sea because of bending of the subducting slab. This results may explain some normal-faulting earthquakes in this region, such as the Pingtung M_W 7.0 earthquake in 2006 (Chen et al. 2008; Lee et al. 2008; Kaus et al. 2009; Sun et al. 2011).

Acknowledgments This study is supported by the National Natural Science Foundation of China (No. 41204066), China Geological Survey (Nos. 12120114002101, 12120114002401), Deep Exploration in China (SinoProbe-08-01, SinoProbe-07), and the CAS/SAFEA International Partnership Program for Creative Research Teams. Thanks are given to Chang-Pai Chang for providing strain rate results. We thank the Broadband Array in Taiwan for Seismology (BATS), the Central Weather Bureau Seismic Network (CWBSN). Some figures were generated with the GMT software. Two anonymous reviewers provide constructive comments for this paper.

Open Access This article is distributed under the terms of the Creative Commons Attribution 4.0 International License (<http://creativecommons.org/licenses/by/4.0/>), which permits unrestricted use, distribution, and reproduction in any medium, provided you give appropriate credit to the original author(s) and the source, provide a link to the Creative Commons license, and indicate if changes were made.

References

- Angelier J, Chang T-Y, Hu J-C, Chang C-P, Siame L, Lee J-C, Deffontaines B, Chu H-T, Lu C-Y (2009) Does extrusion occur at both tips of the Taiwan collision belt? Insights from active deformation studies in the ilan plain and pingtung plain regions. *Tectonophysics* 466:356–376
- Brace WF, Kohlstedt DL (1980) Limits on lithospheric stress imposed by laboratory experiments. *J Geophys Res* 85(B11):6248–6252
- Chang C-P, Angelier J, Huang C-Y (2000) Origin and evolution of a melange: the active plate boundary and suture zone of the longitudinal valley, Taiwan. *Tectonophysics* 325:43–62
- Chang C-P, Chang T-Y, Angelier J, Kao H, Lee J-C, Yu S-B (2003) Strain and stress field in Taiwan oblique convergent system: constraints from gps observation and tectonic data. *Earth Planet Sci Lett* 214:115–127
- Chen YR, Lai YC, Huang YL, Huang BS, Wen KL (2008) Investigation of source depths of the 2006 Pingtung earthquake sequence using a dense array at teleseismic distances. *Terr Atmos Ocean Sci* 19(6):579–588
- Chi W-C, Reed DL, Moore G, Nguyen T, Liu C-S, Lundberg N (2003) Tectonic wedging along the rear of the offshore Taiwan accretionary prism. *Tectonophysics* 374:199–217
- Ching K-E, Rau R-J, Lee J-C, Hu J-C (2007) Contemporary deformation of tectonic escape in sw Taiwan from gps observations, 1995–2005. *Earth Planet Sci Lett* 262:601–619
- Coblentz DD, Richardson RM (1996) Analysis of the South American intraplate stress field. *J Geophys Res* 101(B4):8643–8657
- Demets C, Gordon RG, Argus DF, Stein S (1994) Effect of recent revisions to the geomagnetic reversal time scale on estimates of current plate motions. *Geophys Res Lett* 21(20):2191–2194
- England P, Houseman G (1986) Finite strain calculations of continental deformation 2. Comparison with the India-Asia collision zone. *J Geophys Res* 91(B3):3664–3676
- England P, McKenzie D (1982) A thin viscous sheet model for continental deformation. *Geophys J R Astron Soc* 70(2):295–321
- Houseman G, England P (1986) Finite strain calculations of continental deformation 1. Method and general results for convergent zones. *J Geophys Res* 91(B3):3651–3663
- Hsu Y-J, Segall P, Yu S-B, Kuo L-C, Williams CA (2007) Temporal and spatial variations of post-seismic deformation following the 1999 Chi-Chi, Taiwan earthquake. *Geophys J Int* 169(2):367–379
- Hu J-C, Angelier J, Lee J-C, Chu H-T, Byrne D (1996) Kinematics of convergence, deformation and stress distribution in the Taiwan collision area: 2-D finite-element numerical modeling. *Tectonophysics* 255:243–268
- Hu J-C, Angelier J, Yu S-B (1997) An interpretation of the active deformation of southern Taiwan based on numerical simulation and gps studies. *Tectonophysics* 274:145–169
- Hu JC, Yu SB, Angelier J, Chu HT (2001) Active deformation of Taiwan from gps measurements and numerical simulations. *J Geophys Res* 106(B2):2265–2280
- Kao H, Shen SSI, Ma K-F (1998) Transition from oblique subduction to collision: earthquakes in the southernmost Ryukyu arc-Taiwan region. *J Geophys Res* 103(B4):7211–7229
- Kao H, Huang GC, Liu CS (2000) Transition from oblique subduction to collision in the northern Luzon arc-Taiwan region: constraints from bathymetry and seismic observations. *J Geophys Res* 105(B2):3059–3079
- Kaus BJP, Liu YC, Becker TW, Yuen DA, Shi YL (2009) Lithospheric stress-states predicted from long-term tectonic models: influence of rheology and possible application to Taiwan. *J Asian Earth Sci* 36(1):119–134
- Kim K-H, Chiu J-M, Pujol J, Chen K-C, Huang B-S, Yeh Y-H, Shen P (2005) Three-dimensional Vp and Vs structural models associated with the active subduction and collision tectonics in the Taiwan region. *Geophys J Int* 162(1):204–220
- Kirby SH, Kronenberg AK (1987) Rheology of the lithosphere: selected topics. *Rev Geophys* 25(6):1219–1244
- Kubo A, Fukuyama E (2003) Stress field along the Ryukyu Arc and the Okinawa Trough inferred from moment tensors of shallow earthquakes. *Earth Planet Sci Lett* 210:305–316
- Kuo-Chen H, Wu FT, Roecker SW (2012) Three-dimensional P velocity structures of the lithosphere beneath Taiwan from the analysis of TAIGER and related seismic data sets. *J Geophys Res* 117(B6):B06306
- Lacombe O, Mouthereau F, Angelier J, Deffontaines B (2001) Structural, geodetic and seismological evidence for tectonic escape in SW Taiwan. *Tectonophysics* 333:323–345
- Lee SJ, Liang WT, Huang BS (2008) Source mechanisms and rupture processes of the 26 December 2006 Pingtung earthquake doublet as determined from the regional seismic records. *Terr Atmos Oceanic Sci* 19(6):555–566
- Li Q, Liu M, Zhang H (2009) A 3-D viscoelastoplastic model for simulating long-term slip on non-planar faults. *Geophys J Int* 176:293–306
- Lin C-H (2002) Active continental subduction and crustal exhumation: the Taiwan orogeny. *Terra Nova* 14(4):281–287
- Liu M, Yang Y (2003) Extensional collapse of the Tibetan Plateau: results of three-dimensional finite element modeling. *J Geophys Res* 108(B8):2361

- Liu M, Yang Y, Stein S, Zhu Y, Engeln J (2000) Crustal shortening in the andes: why do GPS rates differ from geological rates? *Geophys Res Lett* 27(18):3005–3008
- Ma KF, Song TRA (2004) Thermo-mechanical structure beneath the young orogenic belt of Taiwan. *Tectonophysics* 388:21–31
- Ma K-F, Lee C-T, Tsai Y-B, Shin T-C, Mori J (1999) The Chi-Chi, Taiwan earthquake: large surface displacements on an inland thrust fault. *Eos Trans Am Geophys Union* 80(50):605–611
- Mouthereau F, Petit C (2003) Rheology and strength of the Eurasian continental lithosphere in the foreland of the Taiwan collision belt: constraints from seismicity, flexure, and structural styles. *J Geophys Res* 108(B11):2512
- Mouthereau F, Fillon C, Ma K-F (2009) Distribution of strain rates in the Taiwan orogenic wedge. *Earth Planet Sci Lett* 284:361–385
- Richardson RM (1978) Finite element modeling of stress in the Nazca plate: driving forces and plate boundary earthquakes. *Tectonophysics* 50(2–3):223–248
- Shi YL, Cao JL (2008) Effective viscosity of China continental lithosphere. *Front Earth Sci* 15(3):82–95
- Shin TC, Kuo KW, Lee WHK, Teng TL, Tsai YB (2000) A preliminary report on the 1999 Chi-Chi (Taiwan) earthquake. *Seismol Res Lett* 71(1):24–30
- Shiono K, Sugi N (1985) Life of an oceanic plate: cooling time and assimilation time. *Tectonophysics* 112:35–50
- Sun Y, Zhang H, Shi Y (2011) Numerical investigation on the geodynamical mechanism of the first major shock of 2006 Pingtung M_w 7.0 earthquake. *Sci China Ser D* 54(5):631–639
- Sun Y, Dong S, Fan T, Zhang H, Shi Y (2013) 3D rheological structure of the continental lithosphere beneath China and adjacent regions. *Chin J Geophys* 56(9):2936–2946
- Sun Y, Dong S, Zhang H, Shi Y (2014) Numerical investigation of the geodynamic mechanism for the late Jurassic deformation of the Ordos block and surrounding orogenic belts. *J Asian Earth Sci.* doi:10.1016/j.jseas.2014.08.033
- Tsai Y-B, Teng T-L, Chiu J-M, Liu H-L (1977) Tectonic implications of the seismicity in the Taiwan region. *Mem Geol Soc China* 2:13–41
- Wang C-Y, Shin T-C (1998) Illustrating 100 years of Taiwan seismicity. *Terr Atmos Ocean Sci* 9(4):589–614
- Wu FT, Rau R-J, Salzberg D (1997) Taiwan orogeny: thin-skinned or lithospheric collision? *Tectonophysics* 274:191–220
- Wu Y-M, Chang C-H, Zhao L (2007) Seismic tomography of Taiwan: improved constraints from a dense network of strong motion stations. *J Geophys Res* 112:B08312
- Wu YM, Zhao L, Chang CH, Hsiao NC, Chen YG, Hsu SK (2009) Relocation of the 2006 Pingtung earthquake sequence and seismotectonics in southern Taiwan. *Tectonophysics* 479:19–27
- Yen H-Y, Liang W-T, Kuo B-Y, Yen Y-H, Liu C-S, Reed D, Lundberg N, Su F-C, Chung H-S (1995) A regional gravity map for the subduction-collision zone near Taiwan. *Terr Atmos Ocean Sci* 6(2):233–250
- Yen HY, Yeh YH, Wu FT (1998) Two-dimensional crustal structures of Taiwan from gravity data. *Tectonics* 17(1):104–111
- Yu SB, Kuo LC (2001) Present-day crustal motion along the longitudinal valley fault, eastern Taiwan. *Tectonophysics* 333:199–217
- Yu SB, Chen HY, Kuo LC (1997) Velocity field of GPS stations in the Taiwan area. *Tectonophysics* 274:41–59
- Zhou D, Yu H-S, Xu H-H, Shi X-B, Chou Y-W (2003) Modeling of thermo-rheological structure of lithosphere under the foreland basin and mountain belt of Taiwan. *Tectonophysics* 374:115–134